Received: 15 October 2017 | Revised: 6 March 2018 | Accepted: 6 March 2018

DOI: 10.1002/pip.3012

RESEARCH ARTICLE

WILEY PROGRESS IN PHOTOVOLTAICS

Band gap engineering of atomic layer deposited $Zn_xSn_{1-x}O$ buffer for efficient $Cu(In,Ga)Se_2$ solar cell

Raphael Edem Agbenyeke[1,2] | Soomin Song[3] | Bo Keun Park[1,2] | Gun Hwan Kim[1] | Jae Ho Yun[3] | Taek-Mo Chung[1,2] | Chang Gyoun Kim[1,2] | Jeong Hwan Han[1,4]

[1] Division of Advanced Materials, Korea Research Institute of Chemical Technology (KRICT), 141 Gajeong-Ro, Yuseong-Gu, Daejeon 34114, Republic of Korea

[2] Department of Chemical Convergence Materials, University of Science and Technology (UST), 217, Gajeong-Ro, Yuseong-Gu, Daejeon 34113, Republic of Korea

[3] Photovoltaics Laboratory, Korea Institute of Energy Research (KIER), 152, Gajeong-Ro, Yuseong-Gu,, Daejeon 34113, Republic of Korea

[4] Department of Materials Science and Engineering, Seoul National University of Science and Technology, Seoul 01811, Republic of Korea

Correspondence
Jeong Hwan Han and Chang Gyoun Kim, Division of Advanced Materials, Korea Research Institute of Chemical Technology (KRICT), 141 Gajeong-Ro, Yuseong-Gu, Daejeon 34114, Republic of Korea.
Email: jhan@seoultech.ac.kr; cgkim@krict.re.kr

Funding information
Korea Research Institute of Chemical Technology, Grant/Award Number: SI1803

Abstract

Ternary zinc tin oxide (ZTO) is one of the few environmental compatible buffer materials with the potential of replacing the *n*-CdS buffer in $Cu(In,Ga)Se_2$ (CIGS) solar cells and other photovoltaic systems once its properties are fully understood and optimized. In this work, ZTO films were grown by atomic layer deposition and were logically characterized with the aim of understanding the correlations between compositional changes and film properties. The $ZnO:SnO_2$ pulse ratio significantly affected the growth rate, crystal structure, morphology, and band gap of the ZTO films. By controlling the Sn/(Sn + Zn) atomic ratio, the optical band gap of the ZTO films was tuned between 3.05 and 3.36 eV. Integrating the ZTO films as buffer layers in CIGS solar cells, we observed that films with Sn concentrations of 9 to 16 at.% yielded photo-conversion efficiency close to 14%, which was very comparable to efficiency attained with the commonly used CdS buffer. Furthermore, using X-ray photoelectron spectroscopy analysis, we correlated the current-voltage behavior of the cells to the conduction band offset at the ZTO/ CIGS interface.

KEYWORDS

atomic layer deposition, band gap bowing, conduction band offset, photo-conversion efficiency, $Zn_{1-x}Sn_xO$

1 | INTRODUCTION

Among the second-generation photovoltaic technologies, $Cu(In,Ga)Se_2$ (CIGS) thin film solar cells have reached an impressive lab-scale power conversion efficiency of 22.6%,[1] and the various ongoing research activities promise to push the efficiency even higher. More importantly, the continuous decrease in manufacturing cost is rendering CIGS solar cell very competitive to crystalline silicon solar cells. However, there still remain many challenges that hinder the global commercialization of the CIGS technology, including the *n*-type cadmium sulfide (CdS) used as buffer layer. The narrow band gap of CdS results in parasitic absorption of high-energy photons, which reduces the photo-generated current of the cells.[2,3] In addition, the toxicity of cadmium raises major health and environmental concerns forcing many countries to place bans on the importation and use of the technology.[4] Furthermore, CdS buffer layer is deposited by a nonvacuum chemical bath deposition process, and although the chemical bath deposition process offers a number of advantages including altering the CIGS interface to enhance device performance,[2] it presents a major drawback in adopting a continuous vacuum-based process for large-scale cell/module fabrication.[5] For these reasons, alternative cheap, environmentally friendly and equally efficient buffers are being explored to replace CdS. In_2S_3,[5,6] Zn(O,S)/ZnS,[7-10] ZnMgO,[11] and $Zn_{1-x}Sn_xO_y$ (ZTO)[12] are a few of the actively studied buffer materials. Among them, ZTO has attracted much attention because of the abundance of its constituent elements, its large tunable band gap, and good stability.[13-15] Zinc tin oxide films have also been applied as transparent conducting oxides in organic light-emitting diode,[15] active channel layer in thin film transistor,[16] gas sensors[17,18] and photocatalysts.[19] However, as a buffer layer for solar cells, not many studies have been dedicated to engineering the electronic band structure at the heterojunction interface between *n*-ZTO and *p*-CIGS or other *p*-type absorbers.

Herein, the growth characteristics of ZTO thin films were investigated by using atomic layer deposition (ALD). We observed a strong relationship between film composition and properties, including growth rate, crystallinity, morphology, and optical band gap. Applying the ZTO films as buffer layers for CIGS solar cells, it was found that the flexible tunability in band gap via composition control played an important role in defining the conduction band offset (CBO) formed at the ZTO/CIGS interface. Small amounts of Sn incorporation thus, Sn/(Sn + Zn) atomic percentage between 9 and 16 at.%, yielded CBO < 0. 4 eV and resulted in efficient carrier transport.

2 | EXPERIMENTAL

The ZTO films were grown in a thermal ALD reactor (iPV d100, ISAC Research), using diethyl zinc (DEZ) and bis(1-dimethylamino-2-methyl-2propoxy)tin(II) ($Sn(dmamp)_2$) as the cation sources and 50 wt.% H_2O_2 as the reactant. The films were deposited on *p*-type Si, SiO_2, and soda lime glass substrates over a temperature range of 100–200°C for ex-situ characterization. Prior to the depositions, the $Sn(dmamp)_2$ was heated to 60°C and supplied into the reaction chamber with the aid of Ar carrier gas at a flow rate of 100 sccm, while DEZ was kept at room temperature and supplied into the reaction chamber without a carrier gas. The ALD process conditions for the binary oxides (ZnO and SnO_2) were optimized at 120°C. The optimized pulse sequence for ZnO and SnO_2 ALD were 0.2 second (DEZ pulse)-10 seconds (Ar purge)-0.1 second (H_2O_2 pulse)-10 seconds (Ar purge) and 5 seconds ($Sn(dmamp)_2$ pulse)-5 seconds (Ar purge)-2 seconds (H_2O_2 pulse)-10 seconds (Ar purge), respectively. Ternary ZTO films were deposited by repeating ALD supercycles comprised of *n* subcycles of ZnO ALD and *m* subcycles of SnO_2 ALD. Film thicknesses were measured by using a spectroscopic ellipsometer (Horiba Jobin Yvon UVISEL) with a xenon light source incident at 70°. Zn and Sn areal densities and atomic percentages were determined by X-ray fluorescence (ARL QUANT'X, Thermo Fisher Scientific). X-ray photoelectron spectrometer (XPS, K-Alpha, Thermo Scientific) with a monochromatic Al Kα X-ray source was used to ascertain the chemical properties of the ZTO films and investigate the valence band offset (VBO) at the ZTO/CIGS interface. The crystallinity of films was investigated by glancing angle X-ray diffraction (Smart-Lab, Rigaku). Optical properties including transmittance, absorbance, and band gap were ascertained by using a UV-visible spectrometer (UV-2550 UV-visible spectrometer, Shimadzu). The surface morphology of the deposited films was observed using field effect scanning electron microscope (FESEM, Sigma HD, Carl Zeiss). I-V characteristics of the CIGS solar cells with ALD ZTO buffer layers were measured by using K201 LAB50 solar simulator (with a K401 CW150 lamp power supply) and sourcemeter (2440 5A, Keithley).

3 | RESULTS AND DISCUSSION

Figure 1A depicts the changes in growth rate and Sn/(Sn + Zn) atomic ratio of ZTO films deposited at 120°C using varied Sn/(Sn + Zn) subcycle ratios. The saturated growth of ZnO from DEZ/H_2O_2 and SnO_2 from $Sn(dmamp)_2/H_2O_2$ are presented in Figure S1. The growth rate of ternary ZTO rapidly declined as the Sn/(Sn + Zn) subcycle ratio increased from ~0.14 nm/cycle for pure ZnO to ~0.038 nm/cycle for ZTO with Sn/(Sn + Zn) subcycle ratio of 0.4, after which it slightly increased to ~0.040 nm/cycle for Sn/(Sn + Zn) subcycle ratios above 0.5. From the Sn/(Sn + Zn) atomic ratio, it was found that the growth rate of the ZTO film drastically reduced to 50% that of pure ZnO with only 10 at.% Sn incorporation. Furthermore, the growth rate of the ZTO films at all subcycle ratios was lower than expected considering the rule of mixtures presented by the dashed line. This discrepancy in the growth rate of ternary oxides in ALD was previously reported by Heo et al.[20] The significant decrease in the growth rate of ternary oxides relative to their binary oxide constituents has been attributed to a number of reasons including reduced initial reactivity of one precursor on the terminated surface of another precursor and/or reduction in surface reactive species such as hydroxyl groups,[21] and etching of one metal oxide by reactions that occur with the introduction of a second precursor.[22] Figure 1B showed the variations in the Zn and Sn precursor chemisorption rates as a function of Sn/(Sn + Zn) subcycle ratio. The chemisorption rate of both precursors declined with increasing Sn/(Sn + Zn) subcycle ratio, which explains the lower growth rate of the ternary ZTO film. Notably, the significantly retarded growth of ZnO on SnO_2 is the dominant factor responsible

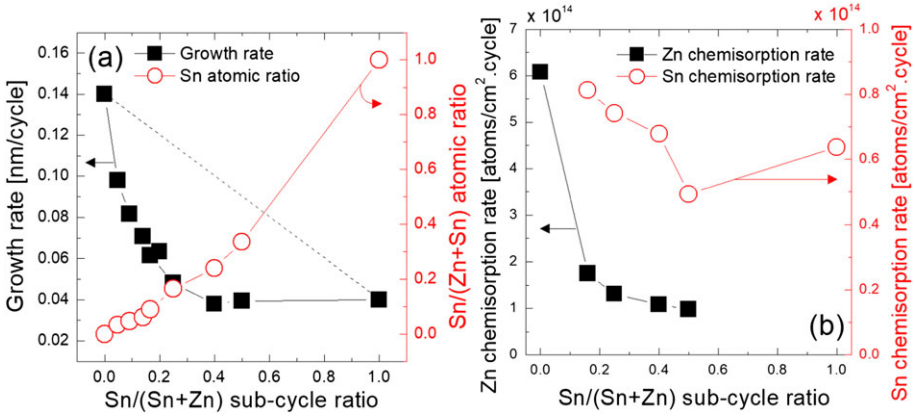

FIGURE 1 A, Growth rate and Sn atomic ratio of ZTO films with increasing SnO_2 subcycle ratio. B, The chemisorption rates of Zn and Sn precursors during ZTO atomic layer deposition at different Sn/(Zn + Sn) subcycle ratios [Colour figure can be viewed at wileyonlinelibrary.com]

for the low growth rate of the ternary oxide, particularly at low Sn concentrations where the most dramatic decreases were observed. Also, considering that the chemisorption rate of Zn is much higher than that of Sn, we can expect that changes in the ZnO growth rate will strongly affect the growth rate of ZTO. A possible reason for the reduced growth (chemisorption) rate of ZnO on SnO_2 is the sluggish reactivity of $Sn(dmamp)_2$ with H_2O_2 at low deposition temperatures. H_2O and H_2O_2 reactant-based ALD processes are well known to exhibit a decreasing growth tendency with increasing temperature due to desorption of OH species from the reaction surface.[23] Here, however, the growth rate of the SnO_2 from $Sn(dmamp)_2/H_2O_2$ increased with growth temperature up to 200°C because of the enhanced reactivity at higher temperatures as shown in Figure S2. The slow reaction kinetics at low temperatures suggests the possibility of unreacted ligands after the SnO_2 cycles, which reduce the available reactive sites for subsequent ZnO growth. A similar contention was made for ZTO films prepared by ALD using DEZ, tetrakis(dimethylamino)tin, and H_2O where dimethylamine ligands were still detected on the reaction surface even after extremely long H_2O pulses (900 s).[24] The report however argued that unremoved ligands only exist on the immediate growing surface and therefore are not incorporated in the films, as a consequence resulting in impurity free SnO_2 films. In contrast, SnO_2 films deposited using $Sn(dmamp)_2$ and H_2O_2 at low temperatures exhibited carbon contaminants within the films implying that ligands were not only on the growing surface but also in the films. More details on the film impurities will be discussed below.

Figure 2A-C depicts the Zn 2p, Sn 3d, and O 1s XP spectra of ZTO films with different Sn/(Sn + Zn) atomic percentages obtained after surface etching. The etching was done by using Ar^+ ion with a beam energy of 2000 eV. All XP spectra were calibrated with the adventitious C 1s peak at 284.5 eV. Irrespective of Sn/(Sn + Zn) atomic percent, the detected Zn $2p_{3/2}$ peaks centered at 1021.9 eV corresponding to Zn^{2+}. Meanwhile, the Sn $3d_{5/2}$ peaks were observed at 486.15 eV, indicating an oxidation state of +4 and thus signifying the formation of SnO_2 and not SnO. Here, it should be noted that the pristine oxidation state of the Sn cation in $Sn(dmamp)_2$ is +2. This clearly shows that the central Sn^{2+} ions in the Sn precursor are oxidized during the ALD process owing to the strong oxidizing power of H_2O_2. The result lines up well with an earlier report, which showed the formation of *n*-type SnO_2 when $Sn(dmamp)_2$ was reacted with O_3, which is also a strong oxidant.[25] The chemical state of the binary SnO_x from the $Sn(dmamp)_2/H_2O_2$ ALD was separately confirmed as being Sn^{4+} as shown in Figure S3. We previously reported the growth of *p*-type SnO films by using $Sn(dmamp)_2/H_2O$ in a ALD process; therefore, H_2O_2 was chosen as reactant in this work, to ensure the formation of *n*-type SnO_2 and ZTO, while minimizing chances of absorber surface damage that can be encountered by using a stronger

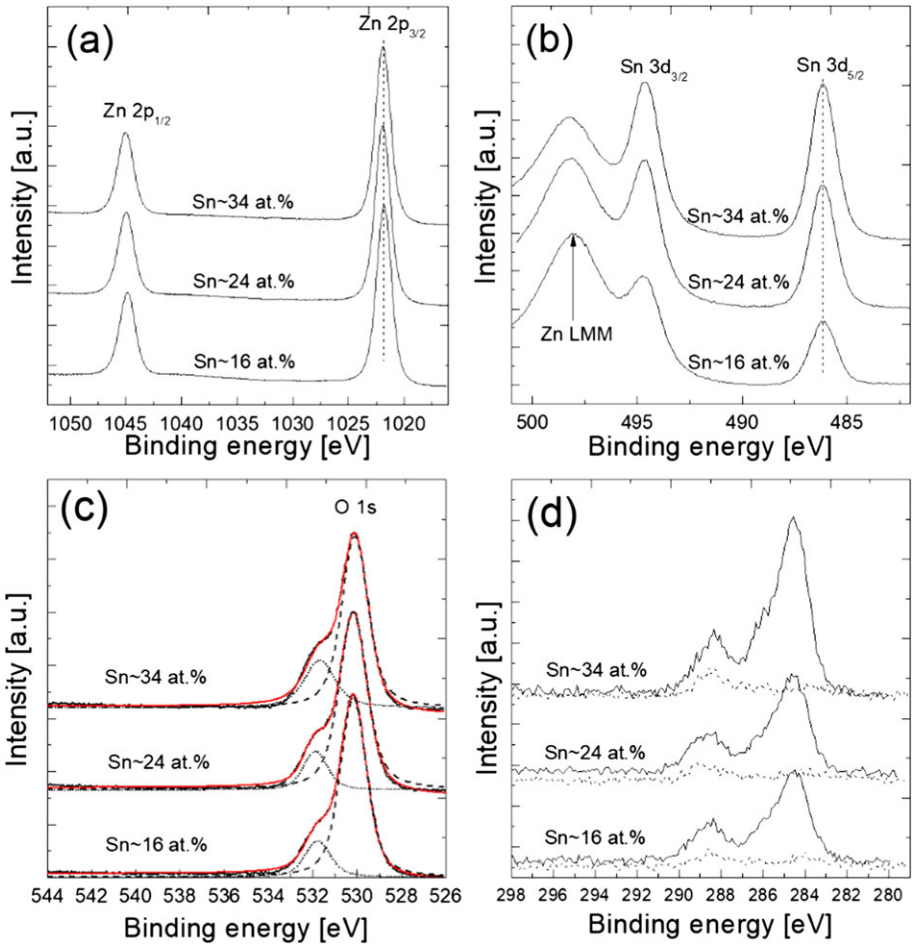

FIGURE 2 XP spectra of (A) Zn 2p, (B) Sn 3d, and (C) O 1s in ZTO films with different Sn/(Sn + Zn) atomic ratios (D) C 1s XP spectra from ZTO films before and after surface sputtering [Colour figure can be viewed at wileyonlinelibrary.com]

reactant-like O_3 when the ZTO buffer is deposited on CIGS absorber layers. Also, in the Sn 3d XP spectra, Zn LMM auger peaks were observed at ~498.2 eV. The intensity of the Sn doublet peak increased relative to the Zn LMM auger peak as the Sn atomic percent increased. The O 1s peak was deconvoluted into 2 peaks centered at 530.2 and 531.8 eV. The peak centered at binding energy 530.2 eV was assigned to lattice oxide,[26] while the peak centered at 531.8 eV was assigned to hydroxides such as Zn-OH and Sn-OH and carbonates.[27] Figure 1D shows a comparison of the C 1s spectra from the different ZTO films before and after surface sputtering. The analysis revealed a noticeable existence of C within the ZTO films even after sputtering. The C peak located ~288.4 eV, which corresponds to carbonates, increased in intensity with Sn atomic concentration. This implies a rather incomplete surface reaction and/or the formation of carbonates during the SnO_2 ALD process. This reasonably correlates with the C impurity concentration found in the pure SnO_2 film, which was as high as 6.3 at.% (Figure S4). X-ray photoelectron spectrometer quantitative analysis of the carbon contents in the ZTO films revealed 1.1, 1.8, and 3.9 at.% of C impurities in 16 Sn at.% ZTO, 24 Sn at.% ZTO, and 34 Sn at.% ZTO films, respectively.

Thirty-nanometer-thick ZTO films deposited on Si substrates were characterized by glancing angle X-ray diffraction to determine the crystal structure. Figure 3 shows the diffraction patterns of ZTO films with different Sn/(Sn + Zn) atomic percentages. Pure ZnO deposited at 120°C exhibited the typical polycrystalline wurtzite structure with peaks at 31.9° (100), 34.4° (002), 36.4° (101), and 56.7° (110), whereas pure SnO_2 deposited at 120°C was amorphous exhibiting no characteristic peaks. In the ternary ZTO films, there was a gradual evolution from a polycrystalline to nanocrystalline/amorphous phase as the Sn/(Sn + Zn) atomic percent increased, implying a steady increase in lattice distortion with Sn incorporation. Above Sn/(Sn + Zn) of 16 at.%, the 3 main ZnO peaks were replaced with a broad peak centered at 34°. This polycrystalline to amorphous/nanocrystalline transformation has been observed in a number of reports on ternary oxides.[14,28-31] Figure S5A-C shows the plan-view SEM images of the ZTO films. All films were dense and free of pinholes. The ZTO film with low Sn atomic concentration of 9 at.% revealed clearly distinct elongated grains, confirming good crystallinity. On the other hand, ZTO films with high Sn concentrations of 24 and 34 at.% exhibited smoother morphologies with less distinguishable grains. The relatively rough film with low Sn concentration could make it a more effective red light scatterer. Since red light has a low absorption coefficient, scattering by the buffer layer could increase the red light path length through the absorber and improve absorption.

To be used as a buffer layer in photovoltaic cells, the selected buffer material should possess a wide band gap to minimize optical losses by allowing majority of the incident light to reach active material. Figure 4 shows the UV-vis characteristics of ZTO films with different Sn/(Sn + Zn) atomic percentages. The films exhibited over 80% transmittance in the visible wavelength range, which is higher than for CdS, which has an absorption edge at around 500 nm due to its narrower band gap.[30] Another attractive feature of the ternary ZTO buffer is its band gap tunability. The band gap of ZTO films was readily controlled by varying the Sn/(Sn + Zn) subcycle ratio. The insert in Figure 4 shows the Sn/(Sn + Zn) atomic percent dependence of the ZTO band gap extracted from the absorption band edges. It reveals a strong parabolic relation known as the band gap bowing effect. The band gap decreased from 3.2 to 3.05 eV and then blue shifted again to 3.36 eV as the Sn/(Sn + Zn) atomic percent increased. A number of factors account for the band gap bowing phenomenon in ternary semiconductor alloys. However, for the ZTO system, a possible explanation for this behavior could be the transition in crystal structure as observed in the XRD analysis or the introduction of localized energy states within the band gap by Sn incorporation,[13] which can effectively alter the band gap.

The ZTO thin films were applied as buffer layers in CIGS solar cells. The cell structure consisted of 1-μm-thick Mo thin films

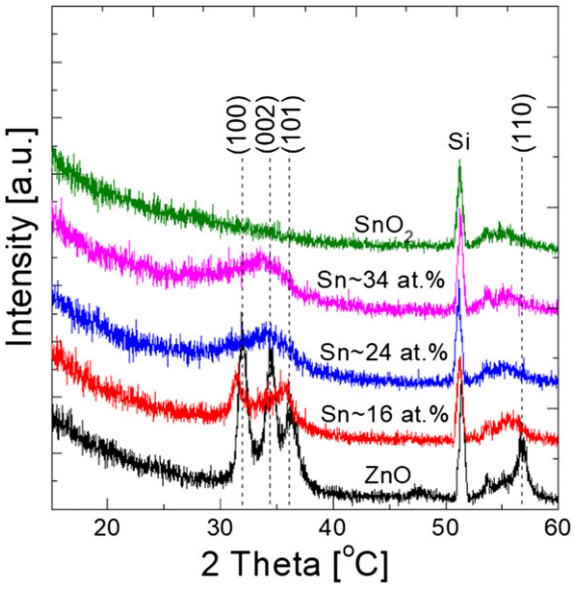

FIGURE 3 Glancing angle X-ray diffraction patterns of ZnO, ZTO, and SnO_2 films deposited at 120°C on Si substrates [Colour figure can be viewed at wileyonlinelibrary.com]

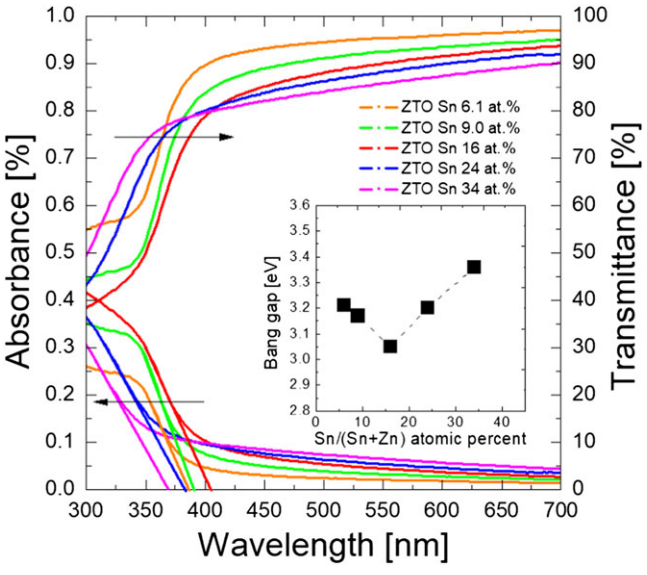

FIGURE 4 Absorbance and transmittance spectra of ZTO films with different Sn/(Sn + Zn) atomic percents. The inset depicts the band gap bowling phenomena of ZTO depending on the Sn atomic percent [Colour figure can be viewed at wileyonlinelibrary.com]

deposited on soda lime glass by DC sputtering, on top of which ~2-μm-thick CIGS films were deposited by evaporation. About 20-nm-thick ZTO films with varied Sn/(Sn + Zn) atomic percentages were deposited on the CIGS absorbers to form the *p-n* heterojunction. Fifty-nanometer-thick i-ZnO and 400-nm-thick AZO films were deposited by RF sputter as TCO, and 400-nm-thick Al was deposited by thermal evaporation as the top electrode. No anti-reflection coatings were applied to the cells. I-V characteristics of the cells with different buffer compositions were measured under AM 1.5G illumination. Figure 5 illustrates the illuminated I-V behavior of cells with ZnO, ZTO and CdS (reference) as buffer layers. For clarity, 2 plots have been indicated. Figure 5A shows the I-V curves of cells with ZTO buffers having Sn atomic percent ≤16 at.% as well as the reference cell, while Figure 5B shows the I-V curves of cells with ZTO buffers having Sn atomic percent ≥16%. In Figure 5A, a continuous enhancement in V_{oc} was observed with the introduction of SnO_2 into the pure ZnO buffer. ZnO is known to exhibit a negative CBO with CIGS,[32,33] which makes it prone to rapid interfacial carrier recombination and generates low V_{oc}. The increase in V_{oc} with the incorporation of SnO_2 denotes a progressive modification of the band alignment from a cliff to a spike type CBO. This proposition was validated by XPS and UV-vis spectroscopy and is discussed in the subsequent part of the report. The V_{oc} peaked at Sn atomic percent between 9% and 16%. The best cell efficiency of 13.9% was obtained with ZTO buffer layer containing 9 Sn at.%, which is comparable to the 14.4% achieved by the CdS reference cell. In contrast to the well-behaved I-V curves observed at low Sn compositions, distorted (S-shaped) curves were obtained for ZTO buffers with Sn atomic concentration >16%. The kink in the curves is indicative of a high-energy barrier height at the CIGS/ZTO interface, which impedes carrier transport and degrades the fill factor as well as the efficiency of the cells.

The thickness of the buffer layer is also an important factor to consider in the cell design. Very thin films can create shunting paths due to complete coverage of the absorber surface, whereas films too thick can generate optical losses and introduce additional series resistances, which affect the FF of the cell. To investigate the effect of the buffer layer thickness on the cell performance, as well as the minimum thickness required to completely cover the CIGS absorber, ZTO film for 16 Sn at.% with varied thickness from 10 to 25 nm with a 5 nm increment were fabricated. As shown in Figure S6, the cells exhibited very similar I-V responses and efficiencies suggesting that within the tested range, the thickness did not significantly affect the cell performance.

The valence and CBOs at the ZTO/CIGS interface were investigated by XPS and UV-vis spectroscopy. For the XPS analysis, ~20-nm-thick ZTO films with varied Sn/(Sn + Zn) atomic percents were deposited on ~2-μm-thick CIGS layers. The samples were sputtered with Ar^+ ion with a low beam energy of 1000 eV for a short etch-time of 15 seconds. The high-resolution valence band spectrum for each etch level was recorded for analysis. The valence band onset values obtained by linear extrapolation of the valence band edges were traced from the ZTO buffer side to the CIGS side as shown in Figure 6A. The valence band onset of the ZTO films was observed around 2 eV, irrespective of cation composition. At the ZTO/CIGS interface, the onset values continuously changed due to band bending until in the CIGS region where it remained constant between 0.45 and 0.48 eV, which correlate well with the value obtained by using ultraviolet photoelectron spectroscopy.[10] The VBO at the ZTO/CIGS heterojunction interface was then determined by using the formula used in the work by Sun et al.[34]

$$\mathrm{VBO} = E_{\mathrm{VB}}^{\mathrm{ZTO}} - E_{\mathrm{VB}}^{\mathrm{CIGS}} + V_{\mathrm{BB}}.$$

$$V_{\mathrm{BB}} = \left(E_{\mathrm{bulk}}^{\mathrm{Cu\ 2p}} - E_{\mathrm{interface}}^{\mathrm{Cu\ 2p}}\right) + \left(E_{\mathrm{interface}}^{\mathrm{Zn\ 2p}} - E_{\mathrm{bulk}}^{\mathrm{Zn\ 2p}}\right)$$

where '$E_{\mathrm{VB}}^{\mathrm{ZTO}}$' and $E_{\mathrm{VB}}^{\mathrm{CIGS}}$ are the valence band onsets of ZTO and CIGS, respectively, and "V_{BB}" is the estimated band bending at the heterojunction interface. The V_{BB} was determined by comparing the shifts in the photoelectron peaks of selected elements in ZTO and CIGS, at the heterojunction interface and in the bulk of the ZTO and CIGS films. Zn 2p photoelectron peak was monitored for the ZTO buffer, while Cu 2p photoelectron peak was monitored for the CIGS absorber. However, because Cu vacancies usually exist at the surface of the CIGS films, In 3d photoelectron peak was used to confirm any observed shifts. The Zn 2p peaks shifted by ~0.1–0.2 eV to lower binding energies at the heterojunction interface relative to the bulk for the different ZTO buffers. However, no such shifts were observed

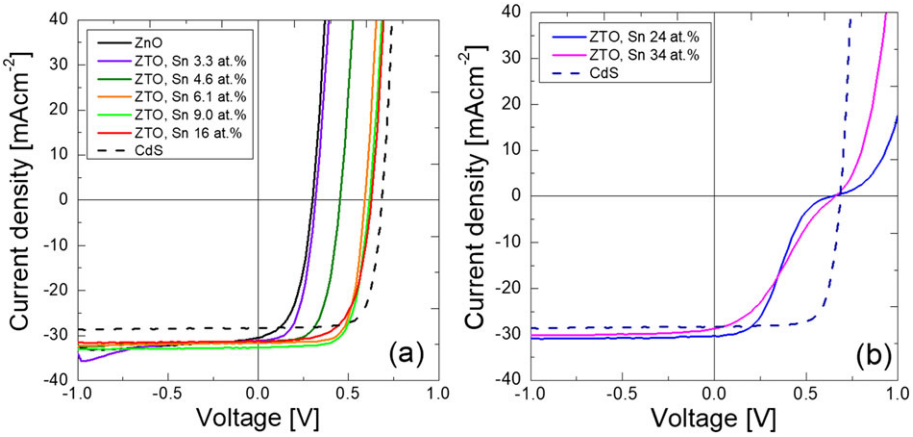

FIGURE 5 Illuminated I-V curves of (A) ZTO films with Sn atomic percent ≤16 at.% and (B) Sn atomic percent ≥24 at.% as well as CdS reference cell [Colour figure can be viewed at wileyonlinelibrary.com]

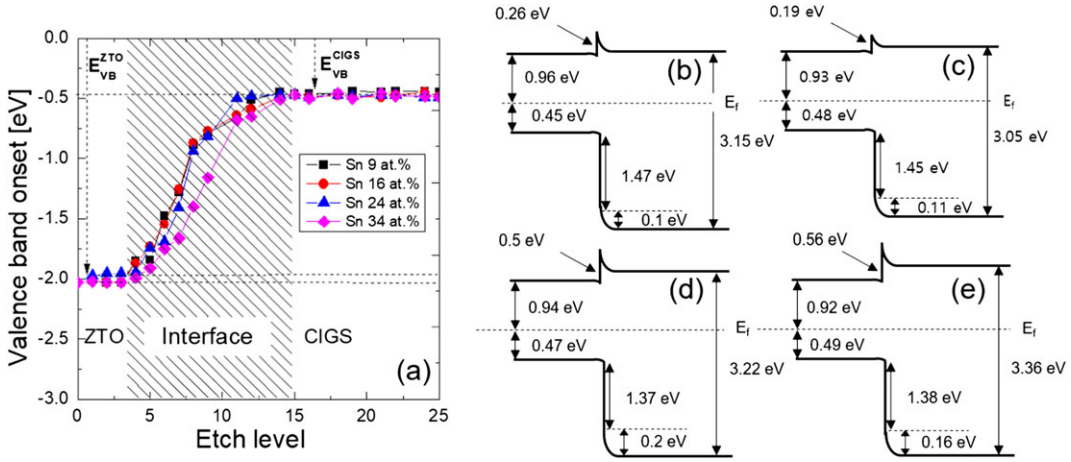

FIGURE 6 A, Trace of the valence band onset of ZTO/CIGS stacks with increasing X-ray photoelectron spectrometer etch level. Schematic band structure at the ZTO/CIGS interface for the different buffer layer compositions of (B) 9 Sn at.%, (C) 16 Sn at.%, (D) 24 Sn at.%, and (E) 34 Sn at.% [Colour figure can be viewed at wileyonlinelibrary.com]

for Cu 2p or In 3d peaks of the CIGS films. This could probably because the shifts were too trivial to be detected by the XPS tool. Hence, the shifts in the Zn 2p were used to estimate the V_{BB}. Next, the surface band gap of the graded CIGS films was quantified by using the equation; $E_g = 1.01 - 1.01x + 1.636x - bx(1 - x)$, where "$x$" is the Ga/(Ga + In) ratio at the surface and "b" is the bowing parameter. "x" was determined from XPS as 0.7 and "b" as 0.21 giving a surface band gap of 1.41 eV. Schematic diagrams of the band alignment at the various *p-n* heterojunction interfaces are displayed in Figure 6B-E. Zinc tin oxide buffers with 9 and 16 Sn at.% exhibited small positive energy barrier heights of 0.19 and 0.26 eV, respectively (Figure 6B, C), which correlates well with their I-V behavior and efficiency. Contrarily, ZTO buffers with Sn compositions of 24 and 34 at.% exhibited high-energy barrier heights of 0.5 and 0.56 eV, respectively (Figure 6D,E), which suggests an inhibition to efficient carrier transport and explains the characteristic "kink" in the I-V curves.

4 | CONCLUSION

Zinc tin oxideternary oxide films were grown by ALD by using DEZ and $Sn(dmamp)_2$ as metal organic precursors and 50 wt.% H_2O_2 as reactant. The growth dynamics for various $ZnO:SnO_2$ subcycles ratios was studied by using ellipsometry and X-ray fluorescence spectroscopy. A significant decrease in the growth rate of the ternary ZTO was observed relative to ZnO and was attributed mainly to the reduced chemisorption/growth rate of ZnO on SnO_2 surface. The ZTO film composition was found to strongly influence film properties including electrical resistivity, lattice arrangement, morphology, and optical band gap. Flexible modulation of the optical band gap of ZTO films via composition control allowed their use as *n*-type buffer layers in CIGS solar cells. The incorporation of Sn significantly improved V_{oc} by modifying the interface band alignment and alleviating interfacial recombination. The best power conversion efficiency of 13.9% was obtained by using ZTO films with Sn atomic concentration ~9 at.%, which was comparable to the 14.4% achieved by the CdS buffer.

ACKNOWLEDGEMENTS

This work was supported by Korea Research Institute of Chemical Technology (SI1803, development of smart chemical materials for IoT device).

CONFLICT OF INTEREST

The authors declare no competing financial interests.

AUTHOR CONTRIBUTIONS

The manuscript was written through contributions of all authors. All authors have given approval to the final version of the manuscript.

ORCID

Jeong Hwan Han http://orcid.org/0000-0002-8314-9235

REFERENCES

1. Schmidt SS, Wolf C, Rodriguez-Alvarez H, et al. Adjusting the Ga grading during fast atmospheric processing of $Cu(In,Ga)Se_2$ solar cell absorber layers using elemental selenium vapor. *Prog Photovolt Res Appl*. 2017;25(5):341-357. https://doi.org/10.1002/pip.2865
2. Schwartz C, Nordlund D, Weng T-C, et al. Electronic structure study of the CdS buffer layer in CIGS solar cells by X-ray absorption spectroscopy: experiment and theory. *Sol Energy Mater Sol Cells*. 2016; 149:275-283.
3. Orgassa K, Rau U, Nguyen Q, Schock HW, Werner JH. Role of the CdS buffer layer as an active optical element in $Cu(In,Ga)Se_2$ thin-film solar cells. *Prog Photovolt Res Appl*. 2002;10(7):457-463. https://doi.org/10.1002/pip.438
4. Directive 2002/95/EC of the European parliament and of the council of 27 January 2003 on the restriction of the use of certain hazardous substances in electrical and electronic equipment. *Off J Eur Union* 2013; L37/19-L37/23.
5. Naghavi1 N, Spiering S, Powalla M, Cavana B, Lincot D. High-efficiency copper indium gallium Diselenide (CIGS) solar cells with indium sulfide buffer layers deposited by atomic layer chemical vapor deposition (ALCVD). *Prog Photovolt Res Appl*. 2003;11(7):437-443. https://doi.org/10.1002/pip.508
6. Sáez-Araoz R, Krammer J, Harndt S, et al. ILGAR In_2S_3 buffer layers for Cd-free $Cu(In,Ga)(S,Se)_2$ solar cells with certified efficiencies above

16%. *Prog Photovolt Res Appl*. 2012;20(7):855-861. https://doi.org/10.1002/pip.2268

7. Wi JH , Kim TG, Kim JW, Lee WJ, Cho DH, Han WS, Chung YD. Photovoltaic performance and Interface behaviors of Cu(In,Ga)Se_2 solar cells with a sputtered-Zn(O,S) buffer layer by high-temperature annealing. *ACS Appl Mater Interfaces* 2015; 7: 17425–17432. https://doi.org/10.1021/acsami.5b04815, 31
8. Mezher M, Garris R, Mansfield LM, et al. Electronic structure of the Zn(O,S)/Cu(In,Ga)Se_2 thin film solar cell interface. *Prog Photovolt Res Appl*. 2016;24(8):1142-1148.
9. Islam MM, Ishizuka S, Yamada A, et al. CIGS solar cell with MBE-grown ZnS buffer layer. *Sol Energy Mater Sol Cells*. 2009;93(6-7):970-972. https://doi.org/10.1016/j.solmat.2008.11.047
10. Larina L, Shin DH, Kim JH, Ahn BT. Alignment of energy levels at the ZnS/Cu(In,Ga)Se_2 interface. *Energ Environ Sci*. 2011;4(9):3487-3493. https://doi.org/10.1039/c1ee01292d
11. Lee CS, Larina L, Shin YM, Al-Ammar EA, Ahn BT. Design of energy band alignment at the $Zn_{1-x}Mg_xO$/Cu(In,Ga)Se_2 interface for Cd-free Cu(In,Ga)Se_2 solar cells. *Phys Chem Chem Phys*. 2012; 14(14):4789-4795.
12. Lindahl J, Zimmermann U, Szaniawski P, Törndahl T, Hultqvist A, Salome P, Platzer-Bjorkman C, Edoff Marika. Inline Cu(In,Ga)Se_2 co-evaporation for high-efficiency solar cells and modules. *IEEE J Photovoltaics* 2013; 3: 1100–1105. DOI: https://doi.org/10.1109/JPHOTOV.2013.2256232, 3
13. Lee YS, Heo J, Siah SC, et al. Ultrathin amorphous zinc-tin-oxide buffer layer for enhancing heterojunction interface quality in metal-oxide solar cells. *Energ Environ Sci*. 2013;6(7):2112-2118. https://doi.org/10.1039/c3ee24461j
14. Wei J, Yin Z, Chen SC, Zheng Q. Low-temperature solution-processed zinc tin oxide film as a cathode interlayer for organic solar cells. *ACS Appl Mater Interfaces*. 2017;9(7):6186–6193-6186–6193, 6193. https://doi.org/10.1021/acsami.6b13724
15. Gorrn P, Ghaffari F, Riedl T, Kowalsky W. Zinc tin oxide based driver for highly transparent active matrix OLED displays. *Solid-State Electron*. 2009;53(3):329-331.
16. Nayak PK, Hedhili MN, Cha D, Alshareef HN. Impact of soft annealing on the performance of solution-processed amorphous zinc tin oxide thin-film transistors. *ACS Appl Mater Interfaces*. 2013;5(9):3587-3590. https://doi.org/10.1021/am303235z
17. Yu JH, Choi GM. Selective CO gas detection of Zn_2SnO_4 gas sensor. *J Electroceram*. 2002;8(3):249-255. https://doi.org/10.1023/A:1020810503321
18. Guoz W. Hollow and porous $ZnSnO_3$ gas sensor for ethanol gas detection. *J Electrochem Soc*. 2016;163(5):131-139. https://doi.org/10.1149/2.0281605jes
19. Danwittayakul S, Jaisai M, Koottatep T, Dutta J. Enhancement of photocatalytic degradation of methyl Orange by supported zinc oxide nanorods/zinc Stannate (ZnO/ZTO) on porous substrates. *Ind Eng Chem Res*. 2013;52(38):13629-13636. https://doi.org/10.1021/ie4019726
20. Heo JY, Liu Y, Sinsermsuksakul P, et al. (Sn,Al)Ox films grown by atomic layer deposition. *J Phys Chem C*. 2011;115:10277-10283. https://doi.org/10.1021/jp202202x
21. Tanskanen JT, Hägglund C, Bent SF. Correlating growth characteristics in atomic layer deposition with precursor molecular structure: the case of zinc tin oxide. *Chem Mater*. 2014;26(9):2795-2802. https://doi.org/10.1021/cm403913r
22. Elam JW, George SM. Growth of ZnO/Al_2O_3 alloy films using atomic deposition techniques. *Chem Mater*. 2003;15(4):1020-1028. https://doi.org/10.1021/cm020607+
23. Han JH, Chung YJ, Park BK, et al. Growth of *p*-type tin(II) monoxide thin films by atomic layer deposition from Bis(1-dimethylamino-2-methyl-2propoxy)tin and H_2O. *Chem Mater*. 2014;26(21):6088-6091. https://doi.org/10.1021/cm503112v
24. Mackus AJM, MacIsaac C, Kim WH. Bent SF. Incomplete elimination of precursor ligands during atomic layer deposition of zinc-oxide, tin-oxide, and zinc-tin-oxide. *J Chem Phys*. 2017;146: 052802(1–11). https://doi.org/10.1063/1.4961459
25. Choi MJ, Cho CJ, Kim KC, et al. SnO_2 thin films grown by atomic layer deposition using a novel Sn precursor. *Appl Surf Sci*. 2014; 320:188-194.
26. Yang BS, Huh MS, Oh S, et al. Role of ZrO_2 incorporation in the suppression of negative bias illumination induced instability in Zn–Sn–O thin film transistors. *Appl Phys Lett*. 2011;98: 122110(1–3):122110. https://doi.org/10.1063/1.3571448
27. Kim MG, Kim HS, Ha YG, et al. High-performance solution-processed amorphous zinc-indium-tin oxide thin-film transistors. *J Am Chem Soc*. 2010;132(30):10352-10364.
28. Mullings MN, Hägglund C, Tanskanen JT, Yee Y, Geyer S, Bent SF. Thin film characterization of zinc tin oxide deposited by thermal atomic layer deposition. *Thin Solid Films*. 2014;556:186-194.
29. Hultqvist A, Platzer-Björkman C, Zimmermann U, Edoff M, Törndahl T. Growth kinetics, properties, performance, and stability of atomic layer deposition Zn–Sn–O buffer layers for Cu(In,Ga)Se_2 solar cells. *Prog Photovolt Res Appl*. 2012;20(7):883-891. https://doi.org/10.1002/pip.1153
30. Kapilashrami M, Kronawitter CX, Törndahl T, et al. Soft X-ray characterization of $Zn_{1-x}Sn_xO_y$ electronic structure for thin film photovoltaics. *Phys Chem Chem Phys*. 2012;14(29):10154-10159. https://doi.org/10.1039/c2cp41394a
31. Banerjee P, Lee WJ, Bae KR, Lee SB, Structural RGW. Electrical, and optical properties of atomic layer deposition Al-doped ZnO films. *J Appl Phys*. 2010;108: 043504(1–7):043504. https://doi.org/10.1063/1.3466987
32. Minemoto T, Hashimoto Y, Satoh T, Negami T, Takakura H, Hamakawa Y. Cu(In,Ga)Se_2 solar cells with controlled conduction band offset of window/Cu(In,Ga)Se_2 layers. *J Appl Phys*. 2001;89(12):8327-8330. https://doi.org/10.1063/1.1366655
33. Törndahl T, Platzer-Björkman C, Kessler J, Edoff M. Atomic layer deposition of $Zn_{1-x}Mg_xO$ buffer layers for Cu(In,Ga)Se_2 solar cells. *Prog Photovolt Res Appl*. 2007;15(3):225-235. https://doi.org/10.1002/pip.733
34. Sun K, Yan C, Liu F, et al. Over 9% efficient kesterite Cu_2ZnSnS_4 solar cell fabricated by using $Zn_{1-x}Cd_xS$ buffer layer. *Adv Energy Mater*. 2016;6: 1600046(1–6). https://doi.org/10.1002/aenm.201600046

SUPPORTING INFORMATION

Additional Supporting Information may be found online in the supporting information tab for this article.

How to cite this article: Agbenyeke RE, Song S, Park BK, et al. Band gap engineering of atomic layer deposited $Zn_xSn_{1-x}O$ buffer for efficient Cu(In,Ga)Se_2 solar cell. *Prog Photovolt Res Appl*. 2018;1–7. https://doi.org/10.1002/pip.3012